Journal of Molecular Catalysis A: Chemical 352 (2012) 38–44

Contents lists available at SciVerse ScienceDirect

Journal of Molecular Catalysis A: Chemical

journal homepage: www.elsevier.com/locate/molcata

In situ generation of superbasic sites on mesoporous ceria and their application in transesterification

Tian-Tian Li, Lin-Bing Sun*, Lu Gong, Xiao-Yan Liu, Xiao-Qin Liu*

State Key Laboratory of Materials-Oriented Chemical Engineering, College of Chemistry and Chemical Engineering, Nanjing University of Technology, Nanjing 210009, China

ARTICLE INFO

Article history:
Received 14 August 2011
Received in revised form
27 September 2011
Accepted 28 September 2011
Available online 5 October 2011

Keywords:
Dimethyl carbonate
Hard template
In situ functionalization
Mesoporous ceria
Solid superbase

ABSTRACT

Mesoporous solid superbases have high potentials for applications as environmentally benign catalysts in diverse reactions, whereas their preparation remains a challenge. In the present study, an in situ functionalization strategy was designed to fabricate mesoporous solid superbases based on the hard-templating synthetic system of mesoporous ceria. Sodium and potassium modified mesoporous ceria (NaMC and KMC) were successfully prepared, and structural and basic properties were characterized by various methods. The obtained materials exhibit well-expressed mesostructure and superbasicity with a high strength of 27.0. The basic solutions (namely NaOH and KOH aqueous solutions) play a double role by removing the silica template SBA-15 and functioning as the guests. Therefore, sodium and potassium can be coated onto mesoporous ceria formed in situ. This strategy allows the fabrication and functionalization of mesoporous ceria in one step, which avoids the destruction of mesoporous ceria in post-modification. The obtained mesoporous solid superbases also exhibit excellent catalytic performance in dimethyl carbonate (DMC) synthesis. The yield of DMC can reach 64.6% in 4 h over NaMC, which is apparently higher than those over the samples derived from post-modification (28.9%), nonmesoporous ceria (10.8%), as well as the conventional solid base magnesia (7.6%).

1. Introduction

Solid superbasic materials are highly promising for applications in environmentally friendly and economical catalytic processes, because they can catalyze diverse reactions under mild conditions and reduce waste production [1]. Among solid bases with different pore structure, mesoporous basic materials have received wide attention recently. The large pore openings of mesoporous solid bases can favor the diffusion of substrates, which avoids coke formation and subsequent deactivation that usually occurs in microporous catalysts [2,3]. Moreover, the reactions involving bulky molecules become possible under the catalysis of mesoporous solid bases. Hence, more and more attention has been paid to the fabrication of solid superbases with mesoporous structure.

In comparison with other candidates with mesostructure, mesoporous silicas are easier to synthesize and have better stability. Since the discovery of mesoporous silica M41S [4], many attempts have been made to generate basic sites on mesoporous silicas, for example, by grafting basic organic groups [5,6] or incorporating nitrogen-containing species [7,8]. These methods lead to the formation of some new kinds of solid bases with mesostructure. However, the basicity of resultant mesoporous materials was relatively weak [9]. Aiming to improve the base strength, metal oxides with strong basicity such as cesium and potassium oxides were introduced to mesoporous silicas including MCM-41 and SBA-15 [10–12]. Unfortunately, the obtained materials exhibited weak basicity and the mesostructure of supports was destroyed due to the reaction of strongly basic oxides with siliceous frameworks [13,14].

In contrast to silica, nonsiliceous oxides alumina and zirconia have better alkali-resistance and are well-known supports for many solid strong bases [15–17]. The reaction of strongly basic species with supports that occurred in silica-derived materials can be avoided. Furthermore, there are vacancies existed on the surface of the alumina and zirconia [18,19]. Cations in basic metal oxides can insert into these vacancies during activation, which plays an important role in the dispersion of metal oxides and generation of strongly basic sites [15,17,20]. The occurrence of nonsiliceous oxides, therefore, affords a nice opportunity for the synthesis of mesoporous superbasic materials [21,22]. To date, various basic oxides including lithium, sodium, potassium, magnesium, and calcium oxides have been loaded on mesoporous alumina or zirconia [20,23–27], leading to the formation of a series of interesting mesoporous solid bases.

Ceria is one of the most important rare earth oxides, and ceria-based materials have found application in a wide range of fields, such as catalysis, fuel cells, gas sensors, as well as optical devices [28–30]. Ceria has a fluorite crystal structure, which is similar to

* Corresponding authors. Tel.: +86 25 83587177; fax: +86 25 83587191.
E-mail addresses: lbsun@njut.edu.cn (L.-B. Sun), liuxq@njut.edu.cn (X.-Q. Liu).

1381-1169/$ – see front matter © 2011 Elsevier B.V. All rights reserved.
doi:10.1016/j.molcata.2011.09.030

that of zirconia (slightly distorted fluorite structure). The presence of vacancies on the surface of ceria has been demonstrated by both theoretical and experimental data [31,32]. As a result, ceria should be an ideal candidate for the preparation of strong solid bases. To the best of our knowledge, nevertheless, very few reports concern the formation of strongly basic sites on ceria, and much less studies on mesoporous ceria. Therefore, it is highly desirable to fabricate new mesoporous strong bases based on mesoporous ceria.

State-of-the-art synthesis of ordered mesoporous materials includes surfactant-directing and hard-templating methods. Each of the method has its merits as well as shortcomings. The former is usually applied to the synthesis of siliceous mesoporous materials, whereas the later replica route is preferred for nonsiliceous mesoporous materials. Owing to its advantages in topological stability, predictability, and controllability during the synthesis procedures, the hard-templating method brings new opportunities for preparing a variety of ordered mesoporous carbons [33], metals [34] and metal oxides with crystalline frameworks [35]. In the present study, we develop an in situ functionalization strategy based on the hard-templating synthetic system of mesoporous ceria. By flexible utilization of basic solution, sodium and potassium-functionalized mesoporous ceria (NaMC and KMC) are successfully prepared. These materials have well-expressed mesostructure and high base strength up to 27.0, exhibiting the characteristic of solid superbase. The basic solution plays a double role by removing the silica template and functioning as the guest. The basic species are thus coated onto mesoporous ceria formed in situ. This strategy permits the fabrication and functionalization of mesoporous ceria in one step, thus framework damage that often takes place in post-modification process can be eluded. Our results also demonstrate that NaMC sample shows excellent basic catalytic performance in dimethyl carbonate (DMC) synthesis via transesterification. The yield of DMC over NaMC sample is obviously higher than that over the samples derived from post-modification and nonmesoporous ceria.

2. Experimental

2.1. Materials preparation

Mesoporous silica template SBA-15 was synthesized as follows. 3 g of triblock copolymer P123 ($EO_{20}PO_{70}EO_{20}$) was dissolved in 22.5 g of water and 90 g of 2 M HCl aqueous solution with stirring at 40 °C. Then 6.38 g of tetraethylorthosilicate was added to the homogeneous solution and stirred at this temperature for 24 h. The resulting gel was transferred to a Teflon-lined autoclave and kept at 140 °C for 24 h. The resulting solid product was filtered, washed, air-dried at room temperature, and calcined at 550 °C in an air flow for 5 h. The obtained mesoporous silica SBA-15 possesses a surface area of 690 $m^2\,g^{-1}$, a pore volume of 1.187 $cm^3\,g^{-1}$, and a pore diameter of 9.2 nm.

Cerium precursor was introduced to silica template by incipient wetness impregnation. 2 mL of a saturated aqueous solution of $Ce(NO_3)_3{\cdot}6H_2O$ were added to 1 g of SBA-15 and the resulting mixture was ground for 10 min in an agate mortar and pestle. The air-dried solid was calcined under an air atmosphere from room temperature to 500 °C with a rate of 2.5 °C min^{-1} and maintained at that temperature for 4 h to convert cerium nitrate to cerium oxide. This procedure was repeated, and the intermediate CeO_2/SBA-15 was formed. CeO_2/SBA-15 was then reacted with 2 M aqueous NaOH solution and 2 M aqueous KOH solution respectively for 24 h. After filtrating and drying in vacuum at 60 °C, the materials NaMC and KMC were produced. Pure mesoporous ceria (MC) was prepared by thoroughly washing the product from the reaction of CeO_2/SBA-15 with NaOH solution using deionized water. To prepare samples with different sodium contents, 1 and 3 M aqueous NaOH solution were used to react with CeO_2/SBA-15. The resultant samples were denoted as NaMC (1 M) and NaMC (3 M), respectively.

As a comparison, two reference samples with the same composition as NaMC were prepared. The first reference sample is sodium-functionalized mesoporous ceria prepared by post-modification (Na/MC). After the dissolution of a certain amount of NaOH in 10 mL of water, 1 g of mesoporous ceria was added. The mixture was stirring at room temperature for 24 h, then water was evaporated and the solid was dried in vacuum at 60 °C. The second reference sample, sodium-modified nonmesoporous ceria (Na/CeO_2), was prepared by impregnating NaOH onto nonmesoporous ceria in a similar process, where nonmesoporous ceria was obtained by calcining $Ce(NO_3)_3{\cdot}6H_2O$ at 500 °C for 4 h.

2.2. Materials characterization

X-ray diffraction (XRD) patterns of the materials were recorded using a Bruker D8 Advance diffractometer with monochromatic Cu Kα radiation in the 2θ range from 0.7° to 8° and 5° to 80° at 40 kV and 30 mA. The average crystallite size was calculated from the (1 1 1) diffraction peak using Scherrer's equation. Transmission electron microscopy (TEM), high-resolution transmission electron microscopy (HRTEM), and selected-area electron diffraction (SAED) experiments were conducted on a JEM-2010 UHR electron microscope operated at 200 kV. N_2 adsorpotion–desorption experiments were carried out using a Belsorp II system at −196 °C. The temperature selected to perform the degasification step was 150 °C. The degasification time was 3 h. The multipoint Brunauer–Emmet–Teller (BET) surface area was estimated over the relative pressure range from 0.04 to 0.20. The total pore volume was calculated using the amount adsorbed at a relative pressure of about 0.99. The pore size distribution of the mesoporous materials was calculated from the adsorption branch by using the Barrett–Joyner–Halenda (BJH) method. The element contents of the composites were measured by an ARL ADVANT'XP X-ray fluorescence (XRF) spectrometer. Fourier transform infrared (IR) measurements were carried out on a Nicolet Nexus 470 spectrometer with a spectra resolution of 2 cm^{-1} using transparent KBr pellets.

The base strength (H_-) of materials was detected by using a series of Hammett indicators [12]. About 100 mg of sample was activated under N_2 with a flow rate of 30 mL min^{-1} at 700 °C for 2 h before test. Then the sample was transferred into cyclohexane under the protection of nitrogen, and two drops of indicator solution were added to the suspension. The color change of the indicator at the solid surface was monitored. The indicators employed included phenolphthalein (H_- = 9.3), 2,4-dinitroaniline (H_- = 15.0), 4-nitroaniline (H_- = 18.4), benzidine (H_- = 22.5), 4-chloroaniline (H_- = 26.5), and aniline (H_- = 27.0). To measure the amount of basic sites, 100 mg of sample after activation was added into 10 mL of aqueous HCl (0.05 M). The sample suspension was shaken for 24 h and the slurry was separated by a centrifuge. The remained acid in liquid phase was titrated with standard base (0.01 M aqueous NaOH) and phenolphthalein was employed as an indicator. The amount of HCl consumed was used to calculate the basicity. Temperature programmed desorption of CO_2 (CO_2-TPD) experiments were conducted on a BELSORP BEL-CAT-A apparatus. The sample was activated at 700 °C for 2 h prior to the adsorption of CO_2 at room temperature. After the physical adsorbed CO_2 was purged by a He flow (99.999%) at room temperature, the sample was heated to 800 °C at the rate of 8 °C min^{-1}, and the CO_2 liberated was detected by an OmniStar mass spectrometer.

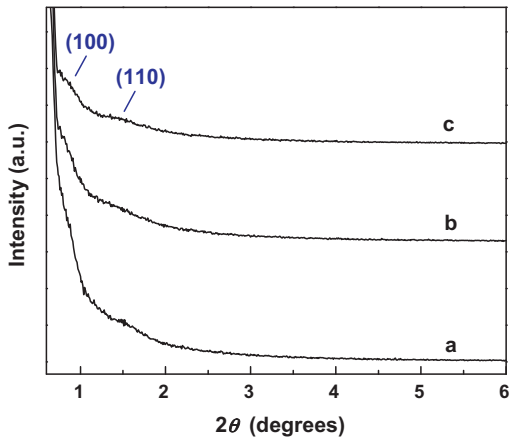

Fig. 1. Low-angle XRD patterns of (a) MC, (b) NaMC, and (c) KMC samples.

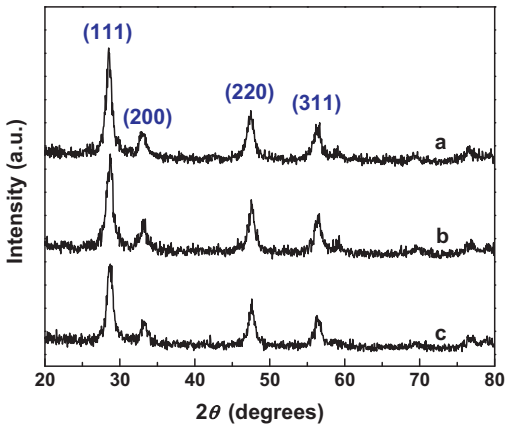

Fig. 2. Wide-angle XRD patterns of (a) MC, (b) NaMC, and (c) KMC samples.

2.3. Catalytic test

Dimethyl carbonate (DMC) was synthesized from the transesterification of ethylene carbonate and methanol. In a typical process, methanol (0.5 mol), ethylene carbonate (0.1 mol), and catalyst (0.5 wt% of methanol) were added to a 50 mL three-necked glass flask with a water-cooled condenser. All the catalysts were pretreated at 700 °C in a N_2 flow (99.999%, 30 mL min^{-1}) for 2 h prior to reaction. The reaction was conducted at 65 °C with stirring for a given period of time. After the reaction was finished, the products and unreacted substrates were recovered from the flask and subjected to centrifuging. The obtained upper liquid was then analyzed by use of a Varian 3800 gas chromatography equipped with a flame ionization detector (FID).

3. Results and discussion

3.1. Structural characterization of materials

Fig. 1 shows the low-angle XRD patterns of MC, NaMC, and KMC samples. The diffraction lines indexed as (1 0 0) and (1 1 0) reflections can be identified, similar to parent SBA-15 shown in Fig. S1. This indicates that the pore regularity of mesoporous silica template is replicated. No obvious decrease of peak intensity takes place after introducing sodium and potassium, which suggests that the in situ functionalization strategy is favorable to the preservation of mesoporous structure. This is apparently different from the sample prepared via post-modification, and no diffraction lines can be observed after loading sodium as will be discussed later.

Fig. 2 presents the wide-angle XRD patterns of different samples. All samples show the diffraction lines at 2θ of 28°, 33°, 47°, and 56°, which can be respectively attributed to the (1 1 1), (2 0 0), (2 2 0), and (3 1 1) reflections of cubic fluorite structured CeO_2 (JCPDS no. 34-394). The broad peak at about 2θ of 23° caused by amorphous silica is not detected in any samples. By comparing the patterns of NaMC and KMC with MC, no additional peaks can be identified. This means that sodium and potassium compounds are well dispersed on mesoporous ceria. Because the intensity of diffraction lines is not strong, the mesoporous walls should be composed of ceria nanoparticles [36]. Further calculation using Scherrer's equation shows that the crystallite size is around 8.3 nm for all samples. It is noticeable that the silica template has a pore diameter of 9.2 nm, which may provide a confined space for the growth of ceria, leading to the formation of uniform crystallite size within the pores.

TEM offers another important technique to characterize periodic ordering of mesostructure. Parent SBA-15 shows an ordered mesostructure as can be seen from Fig. S2. For MC, NaMC, and KMC samples, the images displayed in Fig. 3A–C give direct evidence of ordered mesoporous structure. Furthermore, the introduction of basic species through in situ method does not degrade the symmetry. These results thus confirm the low-angle XRD data shown in Fig. 1. Fig. 3D gives a representative HRTEM image, and some crystallographic planes such as (1 1 1) and (2 0 0) can be identified. These crystallites are randomly oriented in mesoporous frameworks. Meanwhile, some small bridges connected to an array of nanorods can be seen (marked by white arrows). This means that the small channels in SBA-15 were replicated, otherwise separate nanorods would be produced instead of a three-dimensional network [37]. The corresponding SAED pattern (Fig. 3D inset) exhibits four diffuse diffraction rings originated from (1 1 1), (2 0 0), (2 2 0), and (3 1 1) reflections, respectively, which can be indexed by a cubic phase of ceria and is consistent with the results obtained from wide-angle XRD patterns.

Fig. 4A depicts the N_2 adsorption–desorption isotherms of MC, NaMC, and KMC samples. The isotherms can be divided into two parts, namely, a gradual increase in slope starts at a relative pressure of about 0.4 and an intense increase ranging from a relative pressure of 0.9 to 1.0. The upward slope from 0.4 corresponds to capillary condensation with an obvious hysteresis loop, which is the characteristic of mesoporous materials with uniform pore structure. The further increase at higher pressures mirrors interparticle porosity. The existence of such porosity is a common phenomenon in mesoporous materials synthesized via a hard template route [38,39]. As shown in Fig. 4B, all samples display narrow pore size distributions centered at about 4 nm, giving evidence of the well-expressed mesoporosity of the materials. Table 1 lists some structural parameters calculated from isotherms. The sample MC has a BET surface area of 135.2 $m^2 g^{-1}$, which is higher than that reported for mesoporous ceria from surfactant-templating approach (54–119 $m^2 g^{-1}$) [40–42]. The introduction of sodium or potassium results in the decline of both surface area and pore volume, reflecting the location of basic species in the pores of mesoporous ceria.

Fig. 5 gives the IR spectra of different samples. The mesoporous silica template SBA-15 exhibits the bands at 1082 and 805 cm^{-1}, which belongs to asymmetric and symmetric stretching vibration of Si–O–Si frameworks, respectively. The band at 462 cm^{-1} corresponds to the bending vibration of O–Si–O. The band at 960 cm^{-1} is due to the stretching vibration of silanol groups (Si–OH). After the introduction of ceria, all IR bands are reserved despite the reduction of intensity. However, all bands assigned to silica disappear in the spectrum of MC. Together with the absence of silica diffraction lines in wide-angle XRD patterns, it is safe to say that silica template is efficiently removed in the replicated samples. In addition, the

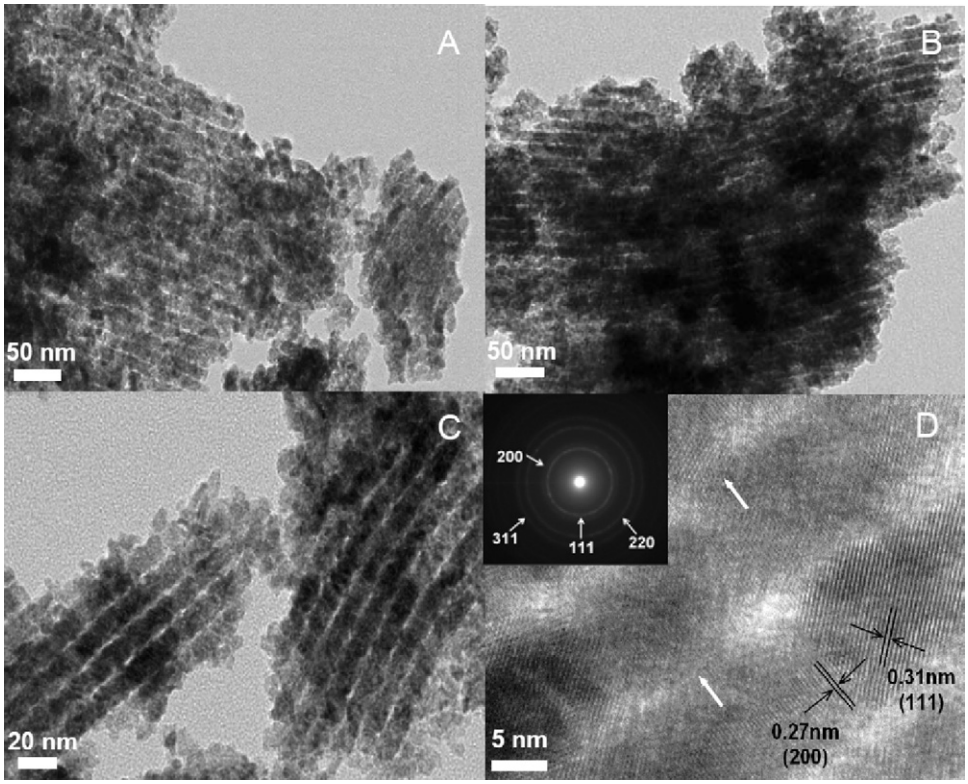

Fig. 3. TEM images of (A) MC, (B) NaMC, and (C) KMC samples as well as HRTEM image of the crystalline framework of (D) MC. Inset in (D) is the SAED pattern of MC.

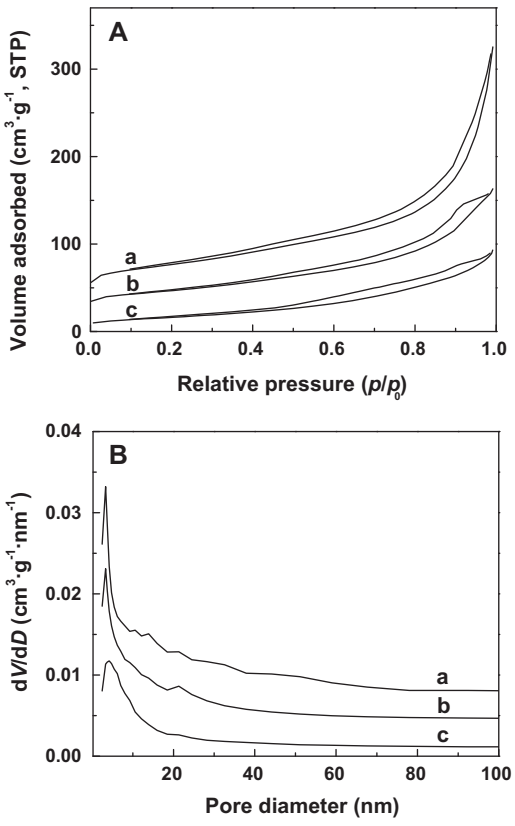

Fig. 4. (A) N_2 adsorption–desorption isotherms and (B) pore size distributions of (a) MC, (b) NaMC, and (c) KMC samples. Curves are offset for clarity.

band ascribed to Ce–O stretching vibration emerges at 475 cm^{-1}, which confirms the formation of ceria [43,44]. For the sample containing sodium and potassium, the IR bands at 1440 cm^{-1} ascribed to surface bicarbonate species with C=O symmetric stretching vibration and 1385 cm^{-1} stemmed from monodentate carbonate species with O–C–O stretching vibration become visible [45–47]. This demonstrates the existence of basic sites on NaMC and KMC samples.

3.2. Basic properties of materials

The basic properties of samples were initially determined by Hammett indicators. As listed in Table 1, a base strength (H_-) of less than 9.3 is detected on sample MC, indicating of the negligible basicity existed on pure mesoporous ceria. It is worth noting that

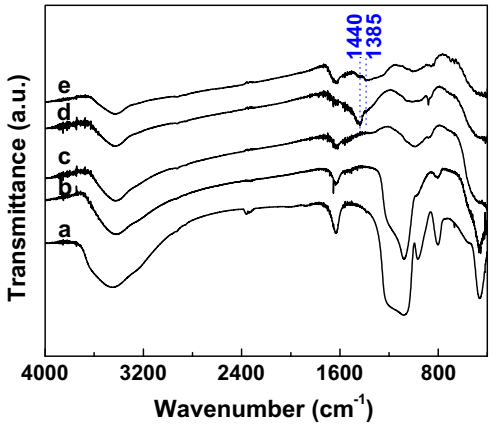

Fig. 5. IR spectra of (a) SBA-15, (b) CeO_2/SBA-15, (c) MC, (d) NaMC, and (e) KMC samples.

Table 1
Physicochemical properties of different samples.

Sample	Metal/Ce[a]	S_{BET}[b] ($m^2\ g^{-1}$)	V_p[b] ($cm^3\ g^{-1}$)	Base strength (H_-)	Amount of basic sites (mmol g^{-1})
MC	0.05	135.2	0.440	<9.3	0.70
NaMC	0.52	92.8	0.203	27.0	2.71
KMC	0.50	59.6	0.149	27.0	2.47
Na/MC	0.52	67.2	0.189	27.0	2.64
Na/CeO_2	0.52	51.1	0.143	27.0	2.59

[a] Detected by XRF; Na/Ce molar ratio for MC, NaMC, Na/MC, and Na/CeO_2, while K/Ce for KMC.
[b] S_{BET}, BET surface area; V_p, total pore volume.

the introduction of sodium leads to a dramatic improvement of base strength. The NaMC sample exhibits a base strength as high as 27.0, which provides the evidence for superbasicity formation according to Tanabe's definition [48]. Similarly, the introduction of potassium generates superbasic sites with a high strength of 27.0 on mesoporous ceria as well. To the best of our knowledge, it is the first report of superbasicity generation on mesoporous ceria.

Table 1 also gives the amount of basic sites in different samples. It is noticeable that the amount of basic sites in MC is as high as 0.70 mmol g^{-1}, despite the negligible content of sodium (Table 1). In order to clarify this phenomenon, the amount of basic sites in pure oxide ceria was measured. Interestingly, the amount of basic sites detected is 0.50 mmol g^{-1}. This suggests that most of the amount of basic sites in MC should derive from ceria support rather than sodium. The introduction of sodium and potassium increases the amount of basic sites obviously. The samples NaMC and KMC possess 2.71 and 2.47 mmol g^{-1} of basic sites, respectively. The amount of basic sites is in line with the content of sodium or potassium (Table 1) after deducting the contribution of ceria support.

The basicity of samples was further investigated by CO_2-TPD. As given in Fig. 6, the sample MC has a weak ability in adsorbing CO_2, and only small desorption appears at low temperatures (around 100 °C). After introducing sodium, the CO_2 desorption peaks at low temperatures enhance apparently. Moreover, an intense peak centered at 620 °C emerges accompanied with a small one at 490 °C. The desorption of CO_2 at such a high temperature of 620 °C can be attributed to the unusually strongly basic sites [12]. This gives further evidence of superbasicity generation on NaMC sample, thus verifying the results of base strength. Similar results can be observed after loading potassium, and both amount and temperature for CO_2 desorbed increase. This indicates the enhancement of both amount and strength of basic sites. In comparison with NaMC, the desorption of CO_2 on KMC appears at a higher temperature of 750 °C, reflecting the stronger basicity of KMC than NaMC. The integration of the peaks in CO_2-TPD patterns of NaMC and KMC was performed. The results showed that the ratio of peak area of NaMC with KMC is 1.2, which is consistent with the ratio of their basic sites amount (1.1, Table 1).

3.3. Catalytic performance

The obtained materials were applied to catalyze the synthesis of DMC via the transesterification of ethylene carbonate and methanol. It is known that DMC is a versatile green chemical, which has been used as carbonylating agent, polar solvent, fuel additive, and methylating agent (instead of methyl halides and dimethyl sulfate, which are both toxic and corrosive) [49–51]. Recently, much attention has been given to the synthesis of DMC over heterogeneous catalysts rather than conventional homogeneous one (for instance sodium methoxide). The catalytic performance of our materials is illustrated in Fig. 7. It can be found that only a tiny amount of DMC (0.4%) is produced over MC after reaction for 4 h. It is worthy of note that the yield of DMC reaches 59.9% at the reaction time of 0.5 h and increases to 64.6% at 4 h under the catalysis of NaMC. As a comparison, a typical solid base magnesia was employed to catalyze the transesterification reaction. Under the same reaction conditions, only 7.6% of DMC was produced at 4 h. This demonstrates the excellent catalytic performance of NaMC sample.

Interestingly, the yield of DMC is only 43.5% at the reaction time of 4 h under the catalysis of KMC, which is obviously lower than that over NaMC. As shown above, the amount of basic sites in NaMC (2.71 mmol g^{-1}) is larger than those in KMC (2.47 mmol g^{-1}), which may lead to a better catalytic performance for NaMC. However, the difference in the amount of basic sites between NaMC and KMC is relatively small, which should not cause such a great difference in catalytic activity. Hence, two other factors should be taken into consideration. The first factor is the difference in surface area. As can be seen from Table 1, the sample NaMC has a

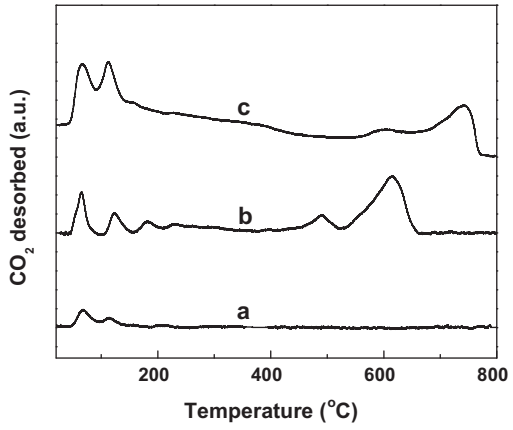

Fig. 6. CO_2-TPD profiles of (a) MC, (b) NaMC, and (c) KMC samples.

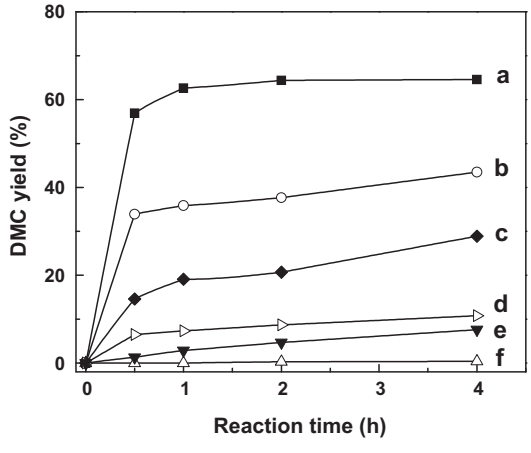

Fig. 7. The yield of DMC under the catalysis of (a) NaMC, (b) KMC, (c) Na/MC, (d) Na/CeO_2, (e) MgO, and (f) MC.

surface area of 92.8 $m^2 g^{-1}$, which is about 36% higher than that of KMC (59.6 $m^2 g^{-1}$). The second factor is the different strength of basic sites. As disclosed by CO_2-TPD results (Fig. 6), the CO_2 desorption peak corresponding to superbasic sites is centered at 620 °C in NaMC, whereas 750 °C in KMC. It should be stated that the samples were activated at 700 °C prior to reaction. This activation temperature is high enough to expose all active sites in NaMC, but only a part of active sites in KMC can be exposed. In order to expose all active sites in KMC, we tried to activate the sample a higher temperature of 750 °C. Unfortunately, the obtained sample exhibited even worse catalytic performance, and the yield of DMC is lower than 5% at 4 h. Further characterization shows that the sample after activated at 750 °C possesses a surface area of 3.1 $m^2 g^{-1}$. Additionally, no diffraction lines can be observed in the low-angle XRD pattern. It can be therefore inferred that the mesostructure of KMC is destroyed at the activation temperature of 750 °C.

To study the effect of sodium content in the samples on the catalytic performance, two additional samples, namely NaMC (1 M) and NaMC (3 M), derived from 1 and 3 M NaOH solution were prepared. Their respective Na/Ce molar ratios are 0.22 and 0.84 (Table S1). The synthesis of DMC catalyzed by NaMC (1 M) and NaMC (3 M) was conducted and the results were shown in Fig. S3. The yields of DMC are 24.3% and 47.5% at 4 h under the catalysis of NaMC (1 M) and NaMC (3 M). Both yields are lower than that over NaMC derived from 2 M NaOH solution (64.6%). The small amount of basic sites (1.14 mmol g^{-1}) as well as weak base strength (22.5) should be responsible for the low DMC yield over NaMC (1 M). The increase of sodium content leads to the improvement of both amount of basic sites (4.22 mmol g^{-1}) and base strength (27.0), while the surface area decreases obviously due to the blockage of pores by sodium species in NaMC (3 M) (Table 1). As a result, the sample NaMC (3 M) exhibits worse catalytic activity as compared with NaMC derived from 2 M NaOH solution.

Two reference samples, that is, Na/MC derived from post-modification and Na/CeO_2 stemmed from nonmesoporous ceria, were also prepared. The surface area of Na/MC is 67.2 $m^2 g^{-1}$, which is obviously lower than that of the sample NaMC prepared from in situ strategy (92.8 $m^2 g^{-1}$). Furthermore, no diffraction lines are observable in low-angle XRD patterns for the Na/MC (data not shown), indicating the destruction of mesostructure in the process of post-modification. The catalytic results in Fig. 7 show that the yield of DMC over Na/MC is only 28.9% at 4 h, which is much lower than that over NaMC (64.6%). According to these results, it is clear that the in situ strategy can avoid the damage of mesoporous structure that occurs in post-modification. This leads to the formation of solid base with well-expressed mesostructure and subsequently good catalytic performance. One may argue that the reaction completed in 2 h for NaMC, however, the yield of DMC over KMC and Na/MC are still increasing. Hence, we prolonged the reaction time to 8 h for these samples. The results show that the yield keeps constant after 4 h (Fig. S4), which confirms the superior catalytic activity of NaMC than KMC and Na/MC. For the reference sample Na/CeO_2, the yield of DMC is only 10.8% at the reaction time of 4 h. The low surface area (51.1 $m^2 g^{-1}$) and nonmesoporous structure should be responsible for such a low catalytic activity.

4. Conclusions

Mesoporous solid superbases, namely sodium and potassium modified mesoporous ceria were fabricated by using an in situ functionalization strategy in the hard template system. These materials have well-expressed mesostructure and superbasicity with a high strength of 27.0. The success of our strategy can be ascribed to the flexible utilization of basic solutions (namely NaOH and KOH aqueous solutions). In addition to removing the silica template, the basic solutions also act as guests and are in situ coated onto the newly formed mesopores. Hence, the fabrication and functionalization of mesoporous ceria can be realized in one step, which avoids the collapse of nonsiliceous mesoporous frameworks in post-modification. Our materials also exhibit excellent basic catalytic performance in the synthesis of DMC via transesterification. The catalytic activity of NaMC sample is apparently better than that over the samples derived from post-modification (Na/MC) and nonmesoporous ceria (Na/CeO_2). The present strategy might open up a route for the synthesis of new mesoporous functional materials.

Acknowledgements

The National Science Foundation of China (nos. 21006048 and 20976082), the Specialized Research Fund for the Doctoral Program of Higher Education of China (no. 20093221120001), the Natural Science Foundation of Jiangsu Province Colleges (no. 09KJB530004), the Major Basic Research Project of Natural Science Foundation of Jiangsu Province Colleges (no. 08KJA530001), China Postdoctoral Science Foundation (no. 20110491406), and the Priority Academic Program Development of Jiangsu Higher Education Institutions are acknowledged for their financial support of this research.

Appendix A. Supplementary data

Supplementary data associated with this article can be found, in the online version, at doi:10.1016/j.molcata.2011.09.030.

References

[1] Y. Ono, J. Catal. 216 (2003) 406–415.
[2] G.J. Wu, S.L. Jiang, L.D. Li, N.J. Guan, Appl. Catal. A: Gen. 391 (2011) 225–233.
[3] L.B. Sun, F.N. Gu, Y. Chun, J.H. Kou, J. Yang, Y. Wang, J.H. Zhu, Z.G. Zou, Micropor. Mesopor. Mater. 116 (2008) 498–503.
[4] C.T. Kresge, M.E. Leonowicz, W.J. Roth, J.C. Vartuli, J.S. Beck, Nature 359 (1992) 710–712.
[5] Y.V.S. Rao, D.E. de Vos, P.A. Jacobs, Angew. Chem. Int. Ed. 36 (1997) 2661–2663.
[6] X. Wang, K.S.K. Lin, J.C.C. Chan, S. Cheng, Chem. Commun. (2004) 2762–2763.
[7] X. Jin, V.V. Balasubramanian, S.T. Selvan, D.P. Sawant, M.A. Chari, G.Q. Lu, A. Vinu, Angew. Chem. Int. Ed. 48 (2009) 7884–7887.
[8] Y. Xia, R. Mokaya, Angew. Chem. Int. Ed. 42 (2003) 2639–2644.
[9] Y.D. Xia, R. Mokaya, J. Phys. Chem. C 112 (2008) 1455–1462.
[10] K.R. Kloetstra, H. van Bekkum, Stud. Surf. Sci. Catal. 105 (1997) 431–438.
[11] Z.Y. Wu, Q. Jiang, Y.M. Wang, H.J. Wang, L.B. Sun, L.Y. Shi, J.H. Xu, Y. Wang, Y. Chun, J.H. Zhu, Chem. Mater. 18 (2006) 4600–4608.
[12] L.B. Sun, J.H. Kou, Y. Chun, J. Yang, F.N. Gu, Y. Wang, J.H. Zhu, Z.G. Zou, Inorg. Chem. 47 (2008) 4199–4208.
[13] Y.H. Sun, L.B. Sun, T.T. Li, X.Q. Liu, J. Phys. Chem. C 114 (2010) 18988–18995.
[14] K.R. Kloetstra, M. van Laren, H. van Bekkum, J. Chem. Soc. 93 (1997) 1211–1220.
[15] L.B. Sun, F.N. Gu, Y. Chun, J. Yang, Y. Wang, J.H. Zhu, J. Phys. Chem. C 112 (2008) 4978–4985.
[16] C. Murugan, H.C. Bajaj, Fuel Process. Technol. 92 (2011) 77–82.
[17] Y. Wang, W.Y. Huang, Y. Chun, J.R. Xia, J.H. Zhu, Chem. Mater. 13 (2001) 670–677.
[18] Y. Chen, L.F. Zhang, Catal. Lett. 12 (1992) 51–62.
[19] Z. Liu, Y. Chen, J. Catal. 177 (1998) 314–324.
[20] L.B. Sun, J. Yang, J.H. Kou, F.N. Gu, Y. Chun, Y. Wang, J.H. Zhu, Z.G. Zou, Angew. Chem. Int. Ed. 47 (2008) 3418–3421.
[21] P. Yang, D. Zhao, D.I. Margolese, B.C. Chmelka, G.D. Stucky, Nature 396 (1998) 152–155.
[22] Z.X. Wu, Q. Li, D. Feng, P.A. Webley, D.Y. Zhao, J. Am. Chem. Soc. 132 (2010) 12042–12050.
[23] Y.Q. Ding, H. Sun, J.Z. Duan, P. Chen, H. Lou, X.M. Zheng, Catal. Commun. 12 (2011) 606–610.
[24] L. Gong, L.B. Sun, Y.H. Sun, T.T. Li, X.Q. Liu, J. Phys. Chem. C 115 (2011) 11633–11640.
[25] L.B. Sun, W.H. Tian, X.Q. Liu, J. Phys. Chem. C 113 (2009) 19172–19178.
[26] S.G. Liu, S.Y. Huang, L.X. Guan, J.P. Li, N. Zhao, W. Wei, Y.H. Sun, Micropor. Mesopor. Mater. 102 (2007) 304–309.
[27] S.G. Liu, J. Ma, L.X. Guan, J.P. Li, W. Wei, Y.H. Sun, Micropor. Mesopor. Mater. 117 (2009) 466–471.
[28] Z.X. Yang, L.G. Xie, D.W. Ma, G.T. Wang, J. Phys. Chem. C 115 (2011) 6730–6740.
[29] D.R. Ou, T. Mori, H. Togasaki, M. Takahashi, F. Ye, J. Drennan, Langmuir 27 (2011) 3859–3866.
[30] D.G. Lamas, M.F. Bianchetti, M.D. Cabezas, N.E. Walsöe de Reca, J. Alloys Compd. 495 (2010) 548–551.
[31] L. Dong, Y. Chen, Chin. J. Catal. 16 (1995) 85–86.

[32] S. Fabris, S.D. Gironcoli, S. Baroni, G. Vicario, G. Balducci, Phys. Rev. B 71 (2005) 041102 (R).
[33] R. Ryoo, S.H. Joo, M. Kruk, M. Jaroniec, Adv. Mater. 13 (2001) 677–681.
[34] K. Lee, Y.H. Kim, S.B. Han, H.K. Kang, S. Park, W.S. Seo, J.T. Park, B. Kim, S.B. Chang, J. Am. Chem. Soc. 125 (2003) 6844–6845.
[35] F. Jiao, A. Harrison, J.C. Jumas, A.V. Chadwick, W. Kockelmann, P.G. Bruce, J. Am. Chem. Soc. 128 (2006) 5468–5474.
[36] S.C. Laha, R. Ryoo, Chem. Commun. (2003) 2138–2139.
[37] K.K. Zhu, H.Y. He, S.H. Xie, X. Zhang, W.Z. Zhou, S.L. Jin, B. Yue, Chem. Phys. Lett. 377 (2003) 317–321.
[38] A. Rumplecker, F. Kleitz, E.L. Salabas, F. Schuth, Chem. Mater. 19 (2007) 485–496.
[39] J. Roggenbuck, G. Koch, M. Tiemann, Chem. Mater. 18 (2006) 4151–4156.
[40] B. Liu, R.T. Baker, J. Mater. Chem. 18 (2008) 5200–5207.
[41] F.B. Gu, Z.H. Wang, D.M. Han, C. Shi, G.S. Guo, Mater. Sci. Eng., B 139 (2007) 62–68.
[42] A. Aranda, B. Puertolas, B. Solsona, S. Agouram, R. Murillo, A.M. Mastral, S.H. Taylor, T. Garcia, Catal. Lett. 134 (2010) 110–117.
[43] T. Mokkelbost, I. Kaus, T. Grsnde, M.A. Einarsrud, Chem. Mater. 16 (2004) 5489–5494.
[44] C. Ho, J.C. Yu, T. Kwong, A.C. Mak, S. Lai, Chem. Mater. 17 (2005) 4514–4522.
[45] L.B. Sun, L. Gong, X.Q. Liu, F.N. Gu, Y. Chun, J.H. Zhu, Catal. Lett. 132 (2009) 218–224.
[46] V.K. Diez, C.R. Apesteguia, J.I. Di Cosimo, J. Catal. 240 (2006) 235–244.
[47] T. Montanaria, L. Castoldib, L. Lietti, G. Busca, Appl. Catal. A 400 (2011) 61–69.
[48] K. Tanabe, R. Noyori, Chokyo-san, Chokyo-enki, Kodansha, Tokyo, 1980.
[49] Y. Ono, Appl. Catal. A 155 (1997) 133–166.
[50] M.A. Pacheco, C.L. Marchall, Energy Fuels 11 (1997) 2–29.
[51] M. Honda, A. Suzuki, B. Noorjahan, K. Fujimoto, K. Suzuki, K. Tomishige, Chem. Commun. (2009) 4596–4598.